metric amount of alkali. The identity of compound **2** was confirmed by using the MIKE spectrum, which is, as required, exactly like those of the m/z 522 ions (see Figure 1). Identical abundances and kinetic energy release[12] values ($T_{1/2}$) in the MIKE spectra of two isobaric ionic species implicate their structural identity.[18]

In conclusion, the data herein reported constitute a strict analogy between the FAB-induced decomposition pathways and solution synthesis. To our knowledge, this is the first example of a retrosynthetic pathway in organometallic chemistry observed under FAB conditions. Furthermore, the identification of highly stable product ions has suggested the possibility of synthesizing these stable species in the condensed phase, which has been successfully performed. Hence FAB mass spectrometry not only has analytical interest but also gives useful information on the stability of different species to be used in the synthesis of new compounds.

Acknowledgment. The financial support from Ministero della Pubblica Istruzione (Rome) is gratefully acknowledged. We thank Walter Ghiotto (Padova) for technical assistance and Antonio Canu (Sassari) for elemental analyses.

Registry No. 1, 58919-44-1; 2, 118299-18-6; 3, 58299-90-4.

(18) Levsen, K.; Schwartz, J. *Angew. Chem., Int. Ed. Engl.* **1976**, *15*, 509.

Organometallic Donor–Acceptor Complexes with Nonplanar Donors: The Zigzag Linear Chain Complex $[(C_6Me_6)_2M^{2+}][iso\text{-}C_4(CN)_6^{2-}]$ (M = Fe, Ru)

Michael D. Ward* and J. C. Calabrese

Central Research and Development Department,† E. I. du Pont de Nemours and Co., Inc., Experimental Station E328, Wilmington, Delaware 19898

Received April 5, 1988

Donor–acceptor solids $[(C_6Me_6)_2Me^{2+}][iso\text{-}C_4(CN)_6^{2-}]\cdot MeNO_2$ (M = Fe, **1a**; M = Ru, **2a**) and $[(C_6Me_3H_3)_2M^{2+}][iso\text{-}C_4(CN)_6^{2-}]$ (M = Fe, **1b**; M = Ru, **2b**) prepared from $(arene)_2M^{2+}$ and $iso\text{-}C_4(CN)_6^{2-}$ are described. Single-crystal X-ray studies show that **1a** crystallizes in the space group $P2_1/c$ with a = 19.875 (6) Å, b = 10.512 (2) Å, c = 15.981 (4) Å, β = 96.65 (3)°, V = 3316 (3) Å^3, ρ = 1.36 g cm^{-3}, Z = 4, R_u = 0.061, and R_w = 0.080. The ruthenium analogue **2a** also crystallizes in the space group $P2_1/c$ with a = 19.973 (2) Å, b = 10.553 (2) Å, c = 16.144 (1) Å, β = 96.80 (7)°, V = 3378 (3) Å^3, ρ = 1.36 g cm^{-3}, Z = 4, R_u = 0.070, and R_w = 0.068. Both complexes exhibit "zigzag" linear chains of closely spaced alternating cations and anions. Donor–acceptor interactions arise from close intermolecular contacts between the C_6Me_6 ligands of the dications and nitrogen atoms of the nonplanar dianion with dianions "bridging" the dications via three of its cyano groups. The complexes exhibit strong charge-transfer bands and are best described as donor–acceptor (DA) complexes with nominally doubly charged ($D^{2-}A^{2+}$) ground states and ($D^{-}A^{+}$) excited states. The difference between the charge-transfer absorption energies of **1** and **2** is equivalent to the difference in the solution reduction potentials of the isostructural $(arene)_2M^{2+}$ cations. The structure of the 19e $(C_6Me_6)_2Fe^{+}$ monocation, reported here for the first time, is essentially identical with that of the 18e dication, suggesting that the charge-transfer transitions of these DA complexes can occur without the formation of energetically unfavorable molecular conformations.

Introduction

Donor–acceptor (DA) interactions in molecular solids are to a large extent the foundation of the extensive interest in these materials.[1] We have been particularly interested in DA solids with organometallic constituents, since the diverse variety of this class of reagents suggests the possibility for systematic investigation of these phenomena as well as the discovery of new materials. Our goal has been to better understand structure-function relationships in these materials, which may result in new concepts for rational modification of structural and electronic properties that are relevent to possible electronic applications.[2]

The structural motif observed for many organic DA complexes[3] and organometallic complexes such $[(C_5H_5)_2Fe^{+}][TCNE^{-}]$[4] and $[(C_5Me_5)_2Fe^{+}][TCNQ^{-}]$[5] consists of mixed stacks of planar π-donors and π-acceptors in a face-to-face arrangement. Similarly, we recently reported $[(C_6Me_3H_3)_2M^{2+}]\{C_3[C(CN)_2]_3^{2-}\}$ (M = Fe, Ru)[6a] complexes which possessed this conventional mixed-stack motif with $(C_6Me_3H_3)_2M^{2+}$ acceptors and $C_3[C(CN)_2]_3^{2-}$ donors, in which the close approach of the π-systems of these species resulted in DA interactions associated with a rather unusual doubly charged "superionic" ground state.[7-9] In contrast, we have recently demonstrated that

† Contribution No. 4593.

(1) *Extended Linear Chain Compounds*; Miller, J. S., Ed.; Plenum Press: New York, 1981–1983; Vols. 1–3.
(2) *Molecular Electronic Devices*; Carter, F., Ed.; Marcel Dekker: New York, 1982.
(3) Herbstein, F. H. *Perspectives in Structural Chemistry*; Dunitz, J. D., Ibers, J. A., Eds.; Wiley: New York, 1971; Vol. IV.
(4) Rosenblum, M.; Fish, R. W.; Bennett, C. *J. Am. Chem. Soc.* **1964**, *86*, 5166.
(5) Candela, G. A.; Swarzendruber, L.; Miller, J. S.; Rice, M. J. *J. Am. Chem. Soc.* **1979**, *101*, 2755.
(6) (a) Ward, M. D. *Organometallics* **1987**, *6*, 754. (b) Ward, M. D.; Miller, J. S., to be submitted for publication.
(7) Mulliken, R. S.; Person, W. B. *Molecular Complexes: A Lecture and Reprint Volume*; Wiley: New York, 1969.
(8) Soos, Z. G. *Annu. Rev. Phys. Chem.* **1974**, *25*, 121.

0276-7333/89/2308-0593$01.50/0

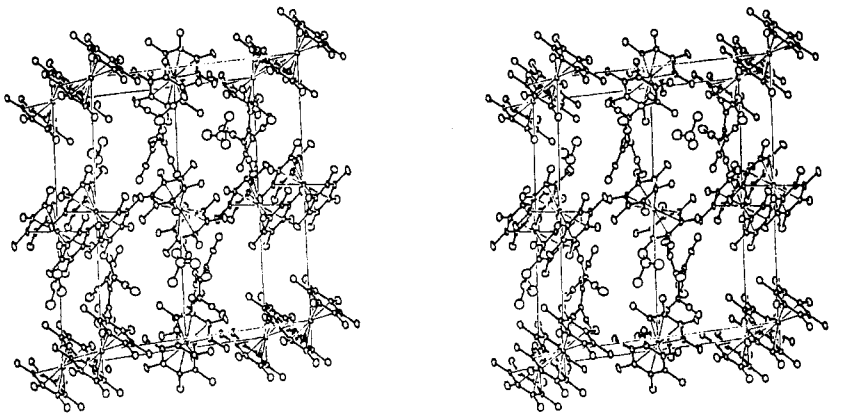

Figure 1. Stereoview of the unit cell of **2a**. Atoms are drawn with 50% elipsoids.

the $(arene)_2M^{2+}$ dications are capable of less conventional motifs in which DA interactions are suggested by close intermolecular contacts between the arene ligands and cyano nitrogen atoms. That is, the charge-transfer complexes $[(C_6Me_6)_2M^{2+}][(TCNQCl_2)^-]_2$ and $[(C_6Me_6)_2M^{2+}][(TCNQF_4)^-]_2$[10] and $[(C_6Me_3H_3)_2M^{2+}][C_3[C(CN)_2]_3^-]_2$[6b] all possessed one-dimensional chains composed of alternating organometallic cations, and polycyanodianion dimers whose molecular planes were essentially *perpendicular* to the arene ligands of the cation rather than face-to-face. Although this type of motif is not common, it is also suggested by the structure of other solids possessing nonplanar constituents, including the organic mixed-stack complex [*N,N*-dimethylbipyridinium^{2+}][*iso*-$C_4(CN)_6^{2-}$][11] and the organometallic complexes $(C_6H_6)Cr(CO)_3$,[12] $[(C_6H_5OMe)Cr(CO)_3][C_6H_3(NO_2)_3]$[13] and [(phenanthrene)$Cr(CO)_3$][$C_6H_3(NO_2)_3$].[14]

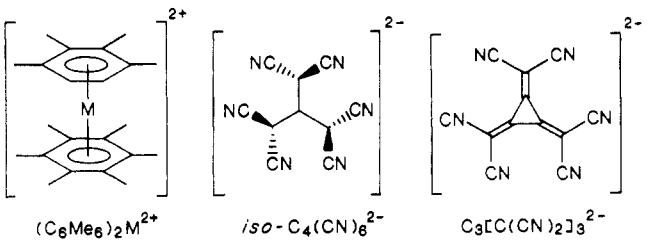

In order to further investigate the donor–acceptor behavior and unusual packing motifs in complexes derived from $(arene)_2M^{2+}$ cations, we have prepared new DA solids derived from $(C_6Me_6)_2M^{2+}$ and the nonplanar $C_4(CN)_6^{2-}$ anion.[15,16] We have found these complexes possess unusual "zigzag" linear chains and exhibit behavior associated with DA interactions between these species, even though face-to-face stacking is not present. The complexes are best described as possessing doubly charged ground states, and as a result the observed charge-transfer transitions are tantamount to electron transfer from the dianion to the organometallic dications. In order to elucidate the structural and electronic requirements of the excited state in these compounds, we have also determined the structure of the 19e $(C_6Me_6)_2Fe^+$ monocation.

Results and Discussion

Synthesis and Structure of $[(arene)_2M^{2+}][iso\text{-}C_4(CN)_6^{2-}]$. When acetonitrile (or nitromethane) solutions of $[n\text{-}Bu_4N^+]_2[iso\text{-}C_4(CN)_6^{2-}]$ are introduced slowly to acetonitrile (or nitromethane) solutions of $[(arene)_2M^{2+}][X^-]_2$ (Me = Fe, X = PF_6; M = Ru, X = BF_4; arene = mesitylene, hexamethylbenzene), air-stable, red-violet needles of $[(arene)_2M^{2+}][iso\text{-}C_4(CN)_6^{2-}]\cdot S$ (**1a**, arene = C_6Me_6; **1b**, arene = $C_6Me_3H_3$; S = acetonitrile or nitromethane) or yellow needles of $[(arene)_2M][C_4(CN)_6]\cdot S$ (**2a**, arene = C_6Me_6; **2b**, arene = $C_6Me_3H_3$; S = acetonitrile or nitromethane) are formed. The microcrystalline solids lose solvent readily, and acceptable elemental analyses of the unsolvated forms are obtained only after thorough removal of solvent in vacuo. The presence of the solvent molecules in **1a** and **2a** was further established by X-ray studies (vide infra). These materials are light sensitive, as exposure to room light for approximately 1 h results in decomposition.

$$[(arene)_2Fe^{2+}][PF_6^-]_2 + [n\text{-}Bu_4N^+]_2[iso\text{-}C_4(CN)_6^{2-}] \xrightarrow{S} [(arene)_2Fe^{2+}][iso\text{-}C_4(CN)_6^{2-}]\cdot S \quad (1)$$

1a: arene = C_6Me_6
1b: arene = $C_6Me_3H_3$
S = CH_3CN, CH_3NO_2

$$[(arene)_2Ru^{2+}][BF_4^-]_2 + [n\text{-}Bu_4N^+]_2[iso\text{-}C_4(CN)_6^{2-}] \xrightarrow{S} [(arene)_2Ru^{2+}][iso\text{-}C_4(CN)_6^{2-}]\cdot S \quad (2)$$

2a: arene = C_6Me_6
2b: arene = $C_6Me_3H_3$
S = CH_3CN, CH_3NO_2

Due to the negligible solubility of these materials, conventional recrystallization methods could not be used to grow single crystals. Therefore, diffusion methods in which the reagents were introduced to each other very slowly were used. This method afforded large crystals of **1a** and **2a**, whereas the mesitylene analogues formed dendritic crystals unsuitable for X-ray analysis.

X-ray Structure of 1a and 2a. Single-crystal X-ray structural analysis revealed that **1a** and **2a** were isomorphous, crystallizing from nitromethane in space group $P2_1/c$ with four ion pairs and four nitromethane molecules per unit cell (Figure 1). The individual cations possess mutually parallel and eclipsed C_6Me_6 ligands, which show no extraordinary deviations from planarity. The C_{ring}–C_{ring} and C_{ring}–C_{methyl} bond distances and angles (Tables I–III;

(9) Andrews, L. J., Keefer, R. M. *Molecular Complexes in Organic Chemistry*; Holden-Day: San Francisco, 1964.
(10) Ward, M. D.; Johnson, D. C. *Inorg. Chem.* **1987**, *26*, 4213.
(11) Nakamura, K.; Kai, Y.; Yasuoka, N.; Kasai, N. *Bull. Chem. Soc. Jpn.* **1981**, *54*, 3300.
(12) (a) Bailey, M. F.; Dahl, L. F. *Inorg. Chem.* **1965**, *4*, 1314. (b) Rees, B.; Coppens, P. *Acta Crystallogr.* **1973**, *B29*, 2515.
(13) (a) Carter, L.; McPhail, A. T.; Sim, G. A. *J. Chem. Soc. A* **1966**, 822. (b) Kobayashi, H.; Kobayashi, K.; Kaizu, Y. *Inorg. Chem.* **1981**, *20*, 4135.
(14) De, R. L.; Von Seyerl, J.; Zsolnai, L.; Huttner, G. *J. Organomet. Chem.* **1979**, *175*, 185.
(15) Middleton, W. J.; Little, E. L.; Coffman, D. D.; Engelhardt, V. A. *J. Am. Chem. Soc.* **1958**, *80*, 2795.
(16) Bekoe, D. A.; Gantzel, P. K.; Trueblood, K. N. *Acta Crystallogr.* **1967**, *22*, 657.

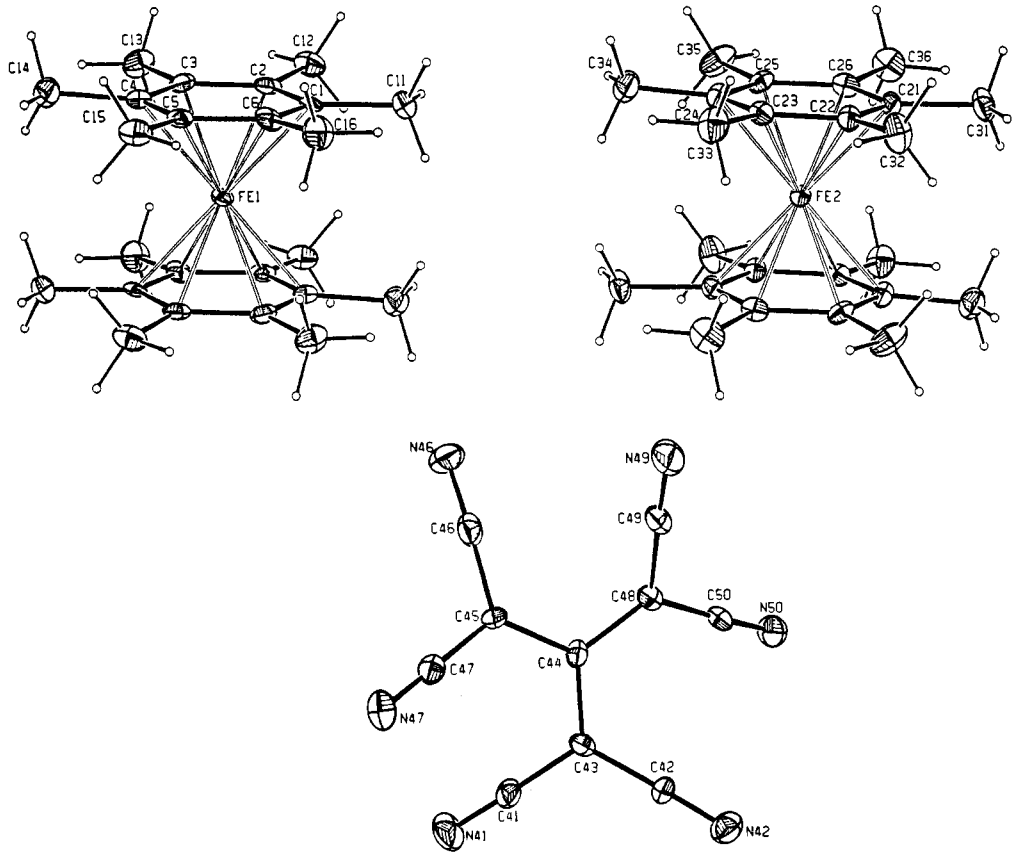

Figure 2. Atom numbering scheme for **1a**. The numbering system is identical for **2a**.

Figure 2) are essentially equivalent for both cations in both **1a** and **2a**. The only substantial differences are in the $M-C_{ring}$ distances due to larger radius of ruthenium compared to iron,[17] resulting in larger intramolecular ligand separations in **2a**. Accordingly, the metal atoms are located 1.63 and 1.75 Å from the centroid of the C_6Me_6 ligand in **1a** and **2a**, respectively, resulting in interligand separations of 3.26 and 3.50 Å. The bond angles are as expected for the aromatic C_6Me_6 ligand. Overall, the structure of the 18e cations are essentially identical with their previously reported structure.[10]

The structural features of the *iso*-$C_4(CN)_6^{2-}$ anions in **1a** and **2a** are essentially identical. The anion is nonplanar due to the twisting of the three $C(CN)_2$ groups out of the internal C_4 plane (Figure 3) that is required to alleviate steric interactions between adjacent cyano groups. This lack of planarity has also been observed in Ca^{2+}[*iso*-$C_4(CN)_6^{2-}$].[17] However, unlike the anion in Ca^{2+}[*iso*-$C_4(CN)_6^{2-}$] which possesses C_3 symmetry, the torsional angles of the $C(CN)_2$ groups with the C_4 plane are all different. The reduced anion symmetry appears to result from the inequivalent intermolecular contacts between the anion and the two unique cations. However, the reduced symmetry does not result in any extraordinary differences in related bond lengths and angles.

The cations and anions form mixed-stack "zigzag" linear chains along the *a* axis in which the *iso*-$C_4(CN)_6^{2-}$ anion "bridges" C_6Me_6 ligands of two unique $(C_6Me_6)_2M^{2+}$ cations. The planes of the two cations form an angle of 93.7°. The angle defined by the centroids of the C_6Me_6 ligands of the cations and the central carbon atom of the anion is 90.9 and 90.2° in **1a** and **2a**, respectively. These chains possess a ...DADA'... repeat unit, where D denotes *iso*-$C_4(CN)_6^{2-}$ and A and A' denote the two unique cations. The anion closely approaches the C_6Me_6 ligands, resulting in very short intermolecular contacts between three of the cyano nitrogen atoms and ring carbon atoms of the C_6Me_6 ligands (Figure 4). The resulting inequivalence of the ring carbon atoms is consistent with solid-state ^{13}C NMR spectra at 100 K.[18] An unusually short contact exists between N47 and C5 of cation I (2.98 Å), with others between N47 and C4 (3.26 Å) and C1 (3.36 Å) and N41 and C3 (3.36 Å). The C_6Me_6 ring of cation II exhibits close contacts between N42 and C25 (3.28 Å) and C24 (3.27 Å), while N41, which is "shared" by both cations, is in close proximity to C21 (3.38 Å). Both N47 and N41 directly overlap carbon atoms of the C_6Me_6 ligands when viewed normal to the ligand planes. Although it does not possess the shortest intermolecular contact, cation II actually resides more closely to centroid of the anion C_4 plane, as it approaches the "flatter" end of the anion. Close contacts between the anion and methyl carbons are also readily observed. However, these are not considered relevant to the donor–acceptor properties of these materials.

The intermolecular interactions and structural motif in **1a** and **2a** are not commonly observed in mixed stack organic[3,19–22] or organometallic[4,5,23,24] DA solids, which generally exhibit face-to-face stacking of planar donors and acceptors with small interplanar distances (i.e., < 3.30 Å). This was also true for $[(C_6Me_3H_3)_2M^{2+}]\{C_3[C(CN)_2]_3^{2-}\}$ (M

(17) Shannon, R. D. *Acta Crystallogr.* **1976**, *A32*, 751.

(18) Ward, M. D.; Farlee, R. D., to be submitted for publication.
(19) *Perspectives in Structural Chemistry*; Dunitz, J. D., Ibers, J. A., Eds.; Wiley: New York, 1971; Vol. IV.
(20) Prout, C. K.; Wright, J. D. *Angew. Chem., Int. Ed. Engl.* **1968**, *7*, 659.
(21) Offen, H. W. *J. Chem. Phys.* **1965**, *42*, 430.
(22) Mayerle, J. J.; Torrance, J. B.; Crowley, J. I. *Acta Crystallogr.* **1979**, *B35*, 2988.
(23) Adman, E.; Rosenblum, M.; Sullivan, S.; Margulis, T. N. *J. Am. Chem. Soc.* **1967**, *89*, 4540.
(24) Sullivan, B. W.; Foxman, B. M. *Organometallics* **1983**, *2*, 187.

Table I. Intramolecular Bond Distances (Å) in $[(C_6Me_6)_2M^{2+}][iso\text{-}C_4(CN)_6^{2-}]\cdot CH_3NO_2$ Complexes[a]

atoms		distance	
		1a	2a
M1	C1	2.163 (5)	2.243 (6)
M1	C2	2.174 (6)	2.260 (5)
M1	C3	2.173 (6)	2.266 (6)
M1	C4	2.167 (6)	2.261 (6)
M1	C5	2.159 (6)	2.263 (5)
M1	C6	2.164 (5)	2.250 (7)
M2	C21	2.151 (5)	2.256 (5)
M2	C22	2.153 (6)	2.242 (7)
M2	C23	2.168 (6)	2.272 (6)
M2	C24	2.170 (5)	2.272 (6)
M2	C25	2.155 (6)	2.258 (5)
M2	C26	2.152 (5)	2.268 (5)
OB	N(solv)	1.49 (3)	1.42 (3)
OA	N(solv)	1.30 (3)	1.57 (3)
N	C(solv)	1.08 (4)	1.09 (4)
N41	C41	1.146 (9)	1.15 (1)
N42	C42	1.130 (9)	1.153 (9)
N46	C46	1.162 (9)	1.161 (9)
N47	C47	1.156 (8)	1.179 (8)
N49	C49	1.123 (9)	1.150 (8)
N50	C50	1.144 (8)	1.144 (7)
C1	C2	1.425 (7)	1.435 (8)
C1	C6	1.428 (6)	1.422 (8)
C1	C11	1.522 (8)	1.526 (9)
C2	C3	1.420 (8)	1.444 (8)
C2	C12	1.492 (9)	1.543 (8)
C3	C4	1.438 (8)	1.432 (7)
C3	C13	1.507 (9)	1.504 (9)
C4	C5	1.410 (8)	1.418 (8)
C4	C14	1.503 (8)	1.517 (8)
C5	C6	1.424 (8)	1.445 (8)
C5	C15	1.496 (8)	1.483 (8)
C6	C16	1.510 (9)	1.516 (9)
C14	C14C	0.970 (7)	0.975 (7)
C21	C22	1.410 (8)	1.446 (8)
C21	C26	1.431 (8)	1.415 (8)
C21	C31	1.512 (8)	1.513 (8)
C22	C23	1.414 (8)	1.425 (9)
C22	C32	1.50 (1)	1.504 (9)
C23	C24	1.408 (8)	1.398 (8)
C23	C33	1.521 (9)	1.517 (8)
C24	C25	1.419 (8)	1.413 (8)
C24	C34	1.487 (9)	1.523 (9)
C25	C26	1.411 (8)	1.414 (8)
C25	C35	1.52 (1)	1.532 (9)
C26	C36	1.516 (8)	1.513 (9)
C41	C43	1.400 (9)	1.434 (8)
C42	C43	1.422 (9)	1.414 (8)
C43	C44	1.423 (9)	1.431 (8)
C44	C45	1.437 (9)	1.430 (8)
C44	C48	1.407 (9)	0.977 (6)
C45	C46	1.409 (9)	1.436 (8)
C45	C47	1.412 (8)	1.384 (9)
C48	C49	1.398 (8)	1.394 (8)
C48	C50	1.457 (8)	1.457 (8)

[a] Numbers in parentheses are estimated standard deviations in the least significant digits.

= Fe, Ru),[6a] in which the anion possessed planar geometry. However, **1a** and **2a** exhibit intermolecular contacts similar to those reported in $(C_6H_6)Cr(CO)_3$[13] and the charge-transfer complexes $[(C_6H_5OMe)Cr(CO)_3][C_6H_3(NO_2)_3]$[14] and $[(phenanthrene)Cr(CO)_3][C_6H_3(NO_2)_3]$.[15] The former was reported to exhibit short contact distances between the carbonyl oxygen atoms and benzene ligand carbon atoms of another $(C_6H_6)Cr(CO)_3$ molecule, whereas the latter two displayed similar intermolecular interactions between the carbonyl oxygen atoms and the trinitrobenzene molecule. Similarly, $[N,N$-dimethylbipyridinium$^{2+}][iso\text{-}C_4(CN)_6^{2-}]$[10] has been reported to possess mixed stacks of cations and anions. This complex also displays short contact distances between the cyano nitrogen atoms and the π-system of N,N-dimethylbipyridinium^{2+} ring, which, although not as short as the contact distances in **1a** and **2a**, are presumably responsible for donor–acceptor interactions that lead to the dark red color of this complex.

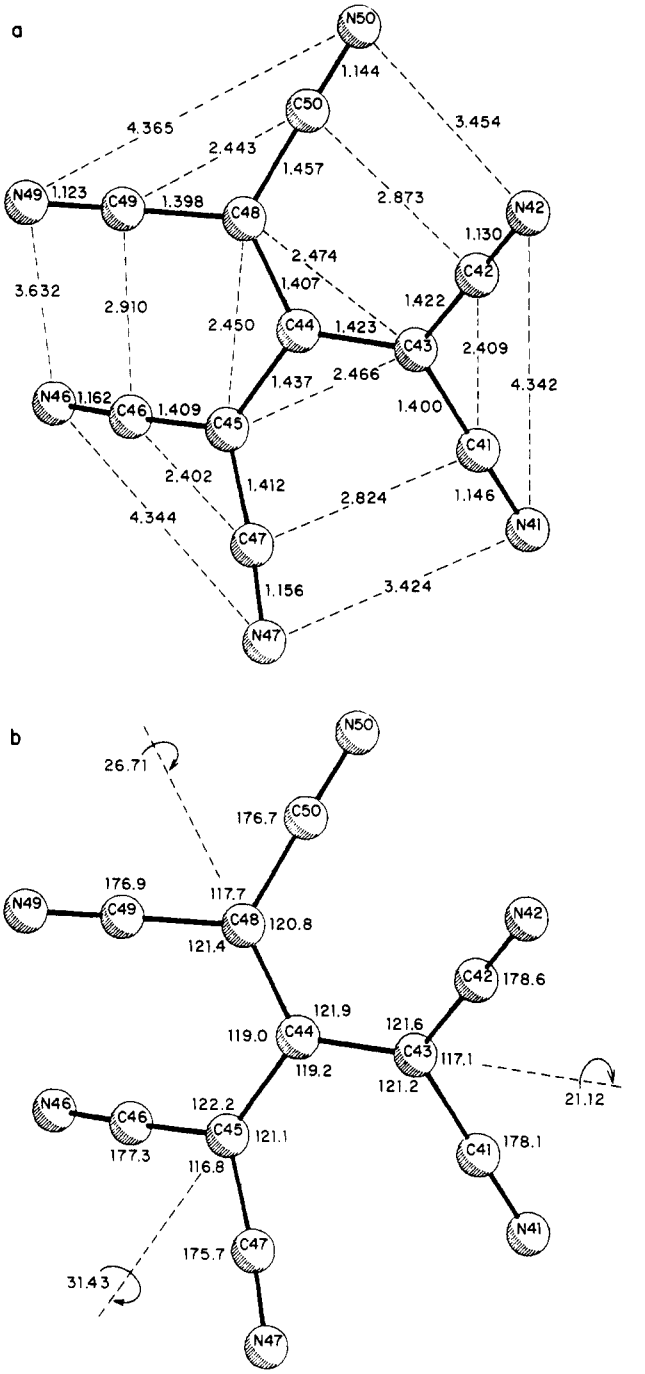

Figure 3. (a) Intramolecular bond distances and interatomic contacts in the anion in **1a**. (b) Intramolecular bond angles in **1a**. The values in **2a** are similar.

Optical Properties. The rather intense colors of **1a,b** and **2a,b**, which are not observed in either the cations or anions alone, are due to charge-transfer transitions observed in the visible region. This behavior is attributed to donor–acceptor interactions resulting from the close approach of the cyano nitrogen atoms of the anions and the ring carbons of the dications. Only small shifts in ν_{CN} of the $iso\text{-}C_4(CN)_6^{2-}$ anion are observed upon complex formation, indicating that the anion in **1** and **2** closely resembles the parent dianion and that the extent of charge transfer in the ground state is not extensive. These solids

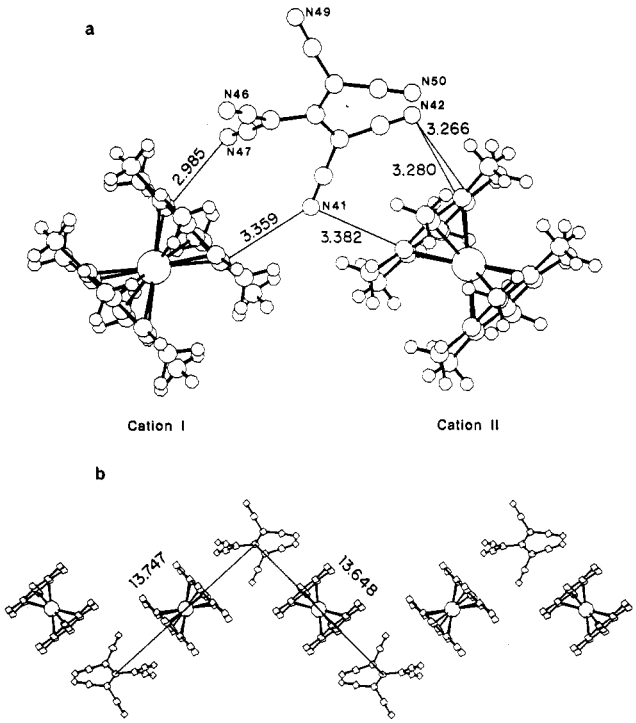

Figure 4. (a) Intermolecular contacts between the two independent $(C_6Me_6)_2Fe^{2+}$ cations and the *iso*-$C_4(CN)_6^{2-}$ anion in **1a**. The values in **2a** are similar. (b) A single linear chain in **1a**. The distance between the central C atoms of the dianions flanking cation II is shorter than that of cation I owing to the different intermolecular overlap of the anion with the two cations.

are thus best described as weak DA complexes possessing ground states with nominally doubly charged donors and acceptors, and singly charged "ionic" excited states similar to behavior previously reported for $[(C_6Me_3H_3)_2M^{2+}]\{C_3[C(CN)_2]_3^{2-}\}$.[6] This assignment is consistent with electrochemical measurements which indicate that the *iso*-$C_4(CN)_6^{2-}$ anion undergoes an irreversible oxidation to the monoanion at potentials that are much more positive than those required for $(arene)_2M^{2+}$ reduction (Table IV); i.e., complete electron transfer from the dianion to the dication is not thermodynamically favored. However, the presence of this redox behavior suggests that the dianion assumes the role as the donor and the organometallic dication the acceptor in the charge-transfer process.[25] Therefore, the charge-transfer transition is tantamount to electron transfer from *iso*-$C_4(CN)_6^{2-}$ to $(C_6Me_3H_3)_2M^{2+}$ (Figure 5). This is consistent with the light-sensitive nature of **1** and **2** as the *iso*-$C_4(CN)_6^{-}$ monoanion is considerably unstable, as evidenced by the irreversible electrochemical oxidation of *iso*-$C_4(CN)_6^{2-}$. The nature of the dication LUMO involved in the CT transition is unclear; however, previous reports suggest that the unoccupied metal e_{1g}^* (d_{xz}, d_{yz}) and ligand e_{2u}^* (p_z) orbitals may be very close in energy,[26,27] and extensive mixing of e_{2u}^* into the metal orbitals was also noted.[28,29] The exact orbital ordering is presently difficult to establish at it is very sensitive to charge as well as substitution on the arene rings, as shown by the systematic cathodic shift in reduction potential as methyl

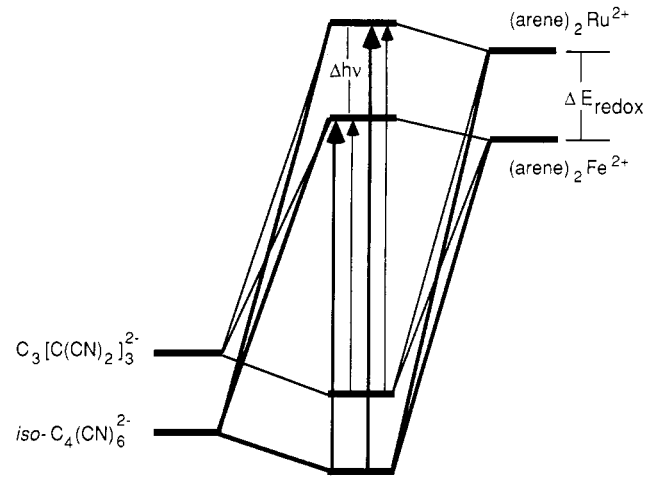

Figure 5. Schematic representation of the charge-transfer transitions responsible for the visible absorptions in **1a** and **2a**. The difference in the redox potentials of the cations (ΔE_{redox}) is nearly equivalent to difference in the charge-transfer transition energies ($\Delta h\nu_{CT}$) for **1a** and **2a**. The tentative relationship of the HOMO of *iso*-$C_4(CN)_6^{2-}$ and $C_3[C(CN)_2]_3^{2-}$ is illustrated by the lower energy (higher ionization potential) of the former. The observed CT absorptions are in accord with this scheme, although the difference in ionization potentials of the two anions cannot be determined from ΔE_{redox} of these anions.

group substitution increases.[30] However, the observation that the C_6H_6 ring of $(C_6H_6)Ru(C_6Me_3H_3)^{2+}$ is readily attacked by hydride[31] is consistent with the presence of a low-lying ligand orbital.

The assignment of the visible absorptions as charge-transfer transitions was corroborated by their observed dependence on the identity of the organometallic acceptor. The charge-transfer energy, $h\nu_{CT}$, is described approximately by eq 3, where EA_A is the electron affinity of the

$$h\nu_{CT} = (IP_D - EA_A) - \langle e^2/r \rangle \quad (3)$$

acceptor, IP_D the ionization potential of the donor, and $\langle e^2/r \rangle$ the difference in Madelung stabilization energy between the ground and excited states. A decrease in the electron affinity of the acceptor therefore results in an increase of the charge-transfer absorption energy. This is clear from a comparison of **1a,b** and **2a,b** where a smaller value of EA_A, as indicated by the more negative reduction potentials of the cations when M = Ru, results in noticeably higher CT transition energies for **2a,b**. Correlations between charge-transfer transition energies and redox potentials of various DA solids have been made previously[32] that indicate that the difference in redox potentials between the donors and acceptors (ΔE_{a-d}) scales somewhat linearly with $h\nu_{CT}$. However, precise agreement between these quantities when comparing series of structurally different donors or acceptors is generally complicated by (a) inequivalent contributions to solvation, which prevents EA_A and IP_D from scaling uniformly with redox potentials, and (b) different Madelung contributions owing to different structures and charge densities. Notably, the difference in the CT absorption energies $\Delta h\nu_{CT}$(**2a** − **1a**) and $\Delta h\nu_{CT}$(**2b** − **1b**) is 0.76 eV, which is essentially equivalent to the measured difference in reduction potential (ΔE_{redox} = 0.77 eV) of these cations in solution[33] (Figure 5). This

(25) Mulliken, R. S. *J. Phys. Chem.* **1952**, *56*, 801.
(26) (a) Anderson, S. E., Jr.; Drago, R. S. *Inorg. Chem.* **1972**, *11*, 1564. (b) Clack, D. W.; Warren, K. D. *J. Organomet. Chem.* **1978**, *152*, C60.
(27) Brintzinger, H.; Palmer, G.; Sands, R. H. *J. Am. Chem. Soc.* **1965**, *87*, 623.
(28) Morrison, W. H.; Ho, E. Y.; Hendrickson, D. N. *Inorg. Chem.* **1975**, *14*, 500.
(29) Anderson, S. E., Jr.; Drago, R. S. *J. Am. Chem. Soc.* **1970**, *92*, 4244.
(30) Hamon, J. R.; Astruc, D.; Michaud, P. *J. Am. Chem. Soc.* **1981**, *103*, 758.
(31) Rybinskaya, M. I.; Kaganovich, V. S.; Kudinov, A. R. *J. Organomet. Chem.* **1982**, *235*, 215.
(32) Torrance, J. B.; Vasquez, J. E.; Mayerle, J. J.; Lee, V. Y. *Phys. Rev. Lett.* **1981**, *46*, 253.

Table II. Positional and Isotropic Thermal Parameters for 1a

atom	x	y	z	B, Å²	atom	x	y	z	B, Å²
Fe1	0.000	0.000	0.000	1.92 (2)	C46	−0.1413 (3)	−0.4778 (5)	0.1104 (4)	3.3 (2)
Fe2	0.500	0.000	0.000	1.79 (2)	C47	−0.1336 (3)	−0.2855 (5)	0.1922 (4)	2.7 (1)
OA	0.2125 (6)	0.528 (1)	0.1503 (8)	7.4 (4)*	C48	−0.2756 (3)	−0.5133 (6)	0.1678 (4)	2.8 (1)
OB	0.259 (1)	0.381 (2)	0.077 (1)	11.9 (6)*	C49	−0.2382 (4)	−0.6204 (5)	0.1967 (5)	3.7 (2)
N	0.276 (1)	0.488 (2)	0.115 (1)	10.4 (6)*	C50	−0.3479 (3)	−0.5297 (4)	0.1428 (4)	3.1 (1)
N41	−0.2393 (4)	−0.0675 (5)	0.1203 (5)	5.9 (2)	H11A	−0.182	0.105	−0.044	5.0*
N42	−0.3919 (3)	−0.2722 (5)	0.2402 (4)	3.7 (1)	H11B	−0.185	0.133	0.052	5.0*
N46	−0.1123 (3)	−0.5505 (7)	0.0732 (4)	4.6 (1)	H11C	−0.133	0.208	0.003	5.0*
N47	−0.0994 (3)	−0.2084 (6)	0.2267 (3)	4.0 (1)	H12A	−0.143	−0.178	−0.126	5.0*
N49	−0.2092 (3)	−0.7058 (6)	0.2232 (5)	6.3 (2)	H12B	−0.197	−0.104	−0.079	5.0*
N50	−0.4039 (3)	−0.5458 (6)	0.1197 (4)	4.1 (1)	H12C	−0.149	−0.029	−0.135	5.0*
C	0.314 (2)	0.560 (3)	0.116 (2)	10.7 (8)*	H13A	−0.015	−0.354	−0.032	5.0*
C1	−0.1023 (2)	0.0243 (4)	0.0309 (3)	2.3 (1)	H13B	−0.093	−0.341	−0.059	5.0*
C2	−0.1004 (3)	−0.0840 (5)	−0.0224 (4)	2.5 (1)	H13C	−0.041	−0.271	−0.117	5.0*
C3	−0.0522 (3)	−0.1817 (6)	−0.0004 (4)	2.5 (1)	H14A	0.071	−0.256	0.151	5.0*
C4	−0.0052 (3)	−0.1709 (6)	0.0747 (4)	2.4 (1)	H14B	0.018	−0.355	0.108	5.0*
C5	−0.0068 (3)	−0.0634 (6)	0.1272 (3)	2.2 (1)	H14C	0.072	−0.292	0.055	5.0*
C6	−0.0562 (3)	0.0331 (5)	0.1061 (3)	2.5 (1)	H15A	0.030	0.029	0.235	5.0*
C11	−0.1553 (3)	0.1270 (7)	0.0083 (4)	4.2 (2)	H15B	0.031	−0.121	0.245	5.0*
C12	−0.1520 (4)	−0.0999 (7)	−0.0972 (4)	3.7 (1)	H15C	0.086	−0.053	0.196	5.0*
C13	−0.0503 (3)	−0.2975 (7)	−0.0557 (4)	3.6 (1)	M16A	−0.098	0.200	0.142	5.0*
C14	0.0432 (3)	−0.2778 (6)	0.0994 (4)	3.8 (2)	H16B	−0.073	0.111	0.219	5.0*
C15	0.0389 (4)	−0.0513 (7)	0.2081 (4)	3.4 (1)	H16C	−0.020	0.189	0.173	5.0*
C16	−0.0623 (3)	0.1434 (7)	0.1652 (4)	4.0 (1)	H31A	0.676	0.136	0.003	5.0*
C21	0.6021 (3)	0.0358 (51)	0.0554 (4)	2.4 (1)	H31B	0.623	0.225	0.042	5.0*
C22	0.6022 (3)	−0.0672 (4)	−0.0011 (4)	2.3 (1)	H31C	0.680	0.153	0.102	5.0*
C23	0.5597 (3)	−0.1732 (6)	0.0070 (3)	2.3 (1)	H32A	0.645	−0.146	−0.099	5.0*
C24	0.5154 (2)	−0.1769 (4)	0.0696 (3)	2.3 (1)	H32B	0.643	0.005	−0.102	5.0*
C25	0.5151 (3)	−0.0735 (6)	0.1266 (4)	2.3 (1)	H32C	0.697	−0.067	−0.037	5.0*
C26	0.5581 (3)	0.0319 (5)	0.1203 (3)	2.4 (1)	H33A	0.531	−0.351	−0.038	5.0*
C31	0.6494 (3)	0.1474 (7)	0.0504 (4)	3.5 (2)	H33B	0.552	−0.259	−0.109	5.0*
C32	0.6512 (4)	−0.0687 (7)	−0.0653 (5)	4.2 (2)	H33C	0.608	−0.322	−0.044	5.0*
C33	0.5629 (4)	−0.2867 (6)	−0.0514 (5)	4.0 (1)	H34A	0.446	−0.278	0.126	5.0*
C34	0.4736 (3)	−0.2920 (7)	0.0800 (5)	4.0 (2)	H34B	0.444	−0.307	0.028	5.0*
C35	0.4700 (4)	−0.0770 (6)	0.1974 (4)	4.3 (2)	H34C	0.503	−0.364	0.093	5.0*
C36	0.5611 (4)	0.1377 (7)	0.1851 (4)	4.0 (1)	N35A	0.476	0.000	0.230	5.0*
C41	−0.2583 (3)	−0.1619 (6)	0.1447 (4)	3.0 (1)	H35B	0.423	−0.085	0.173	5.0*
C42	−0.3432 (3)	−0.2762 (6)	0.2103 (4)	2.6 (1)	H35C	0.482	−0.150	0.233	5.0*
C43	−0.2822 (3)	−0.2784 (6)	0.1717 (4)	2.5 (1)	H36A	0.593	0.202	0.171	5.0*
C44	−0.2450 (3)	−0.3929 (6)	0.1646 (4)	2.3 (1)	H36B	0.516	0.176	0.185	5.0*
C45	−0.1741 (3)	−0.3856 (5)	0.1553 (4)	2.5 (1)	H36C	0.576	0.104	0.241	5.0*

[a] Parameters with an asterisk were refined isotropically.

behavior is identical with that observed for $[(C_6Me_6)_2M^{2+}]\{C_3[C(CN)_2]_3^{2-}\}$ and $[(C_6Me_3H_3)_2M^{2+}]\{C_3[C(CN)_2]_3^{2-}\}$ (M = Fe, Ru; $\Delta h\nu_{CT} = \Delta E_{redox} = 0.77$ eV)[6a] and is attributed to the isomorphous relationship between **1a** and **2a** and, in particular, the isostructural ligand environments about the metal in the cations which mitigates against differences in Madelung energies in the solid state as well as differences in solvation terms associated with their electrochemical reduction in solution.

The larger $h\nu_{CT}$ values of the complexes derived from the $(C_6Me_6)_2M^{2+}$ cations (**1a** and **2a**) are consistent with the more negative redox potentials (i.e. smaller EA_A) of these species compared to the mesitylene analogues. However, they were not as large as one would expect from the difference between the reduction potentials of $(C_6Me_6)_2M^{2+}$ and $(C_6Me_3H_3)_2M^{2+}$ for a given metal. Methyl substitution of the arene ligands appears to unpredictably affect either contributions to solvation terms associated with cation reduction or solid-state Madelung terms, so that quantitative correlation of $\Delta h\nu_{CT}$ and ΔE_{redox} cannot be realized. Indeed, the $[(C_6Me_6)_2M^{2+}]\{C_3[C(CN)_2]_3^{2-}\}$ complexes showed the reverse trend, with the mesitylene complexes exhibiting higher CT energies. However, it should be noted that these comparisons are tenuous since the solid-state structures of all the complexes are not known.

(33) In order to eliminate errors, the reduction potentials of the cations were determined simultaneously.

Changes in the ionization potential of the donor also affect the charge transfer absorption energy. The irreversible oxidation wave at $E_{1/2} = +0.920$ V observed for the *iso*-$C_4(CN)_6^{2-}$ anion suggests a larger ionization potential than that of $C_3[C(CN)_2]_3^{2-}$ ($E° = +0.425$ V vs Ag/AgCl). This results in the larger charge transfer absorption energy of **1a,b** and **2a,b** compared to their $[(arene)_2M^{2+}]\{C_3[C(CN)_2]_3^{2-}\}$ analogues (Figure 5). However, the difference in $h\nu_{CT}$ (Table IV) is significantly larger than the difference in the oxidations potentials (ca. 0.49 V). This reflects the difficulty in correlating $h\nu_{CT}$ with electrochemical properties when isomorphism does not exist and the molecular geometry of the constituents is significantly different.

The extent of charge-transfer interaction, or excited-state mixing, in the ground state of DA solids is commonly estimated from shifts in vibrational frequencies of functional groups belonging to the components, assuming a linear relationship between the degree of charge transfer and the vibrational frequencies.[34,35] The ν_{CN} values of the *iso*-$C_4(CN)_6^{2-}$ anion in **1a,b** and **2a,b** were shifted slightly to higher energy compared to the parent dianion, toward the expected ν_{CN} for the monoanion, suggesting a small

(34) Van Duyne, R. P.; Cape, T. W.; Suchanski, M. R.; Siedle, A. R. *J. Phys. Chem.* **1986**, *90*, 739.

(35) Friedrich, H. B.; Person, W. B. *J. Chem. Phys.* **1966**, *44*, 2161. Jurgensen, C. W.; Peanasky, M. J.; Drickamer, H. G. *J. Chem. Phys.* **1985**, *83*, 6108.

Table III. Positional and Isotropic Thermal Parameters for 2a

atom	x	y	z	B, Å²	atom	x	y	z	B, Å²
Ru1	0.000	0.000	0.000	2.24 (1)	C46	−0.1414 (3)	−0.4812 (6)	0.1106 (4)	3.8 (1)
Ru2	0.500	0.000	0.000	2.20 (1)	C47	−0.1339 (3)	−0.2911 (6)	0.1944 (4)	3.2 (1)
OB	0.2599 (8)	0.382 (2)	0.066 (1)	9.4 (4)*	C48	−0.2771 (3)	−0.5169 (5)	0.1687 (4)	2.9 (1)
OA	0.2105 (7)	0.529 (1)	0.147 (1)	8.0 (3)*	C49	−0.2388 (4)	−0.6263 (6)	0.1973 (5)	4.2 (1)
N	0.277 (1)	0.496 (2)	0.111 (1)	8.9 (5)*	C50	−0.3476 (3)	−0.5360 (6)	0.1447 (4)	3.5 (1)
N41	−0.2378 (4)	−0.0691 (6)	0.1280 (5)	6.3 (2)	H11A	−0.184	0.098	−0.040	5.0*
N42	−0.3896 (3)	−0.2796 (5)	0.2449 (3)	4.4 (1)	H11B	−0.187	0.123	0.056	5.0*
N46	−0.1662 (3)	−0.5560 (6)	0.0716 (4)	5.3 (1)	H11C	−0.136	0.200	0.008	5.0*
N47	−0.0974 (3)	−0.2151 (5)	0.2288 (3)	4.4 (1)	H12A	−0.147	−0.184	−0.126	5.0*
N49	−0.2081 (4)	−0.7116 (6)	0.2251 (5)	6.5 (2)	H12B	−0.200	−0.109	−0.080	5.0*
N50	−0.4034 (2)	−0.5497 (6)	0.1214 (4)	4.2 (1)	H12C	−0.153	−0.034	−0.134	5.0*
C	0.316 (1)	0.568 (2)	0.114 (1)	8.1 (5)*	H13A	−0.015	−0.360	−0.030	5.0*
C1	−0.1054 (3)	0.0162 (5)	0.0339 (4)	2.6 (1)	H13B	−0.094	−0.349	−0.058	5.0*
C2	−0.1030 (3)	−0.0915 (5)	−0.0200 (3)	2.5 (1)	H13C	−0.042	−0.278	−0.109	5.0*
C3	−0.0534 (3)	−0.1893 (6)	0.0012 (3)	3.1 (1)	H14A	0.071	−0.260	0.152	5.0*
C4	−0.0079 (3)	−0.1779 (5)	0.0763 (4)	2.7 (1)	H14B	0.020	−0.361	0.106	5.0*
C5	−0.0095 (3)	−0.0720 (5)	0.1302 (3)	2.5 (1)	H14C	0.073	−0.291	0.056	5.0*
C6	−0.0599 (3)	0.0243 (6)	0.1084 (4)	3.1 (1)	H15A	0.028	0.019	0.236	5.0*
C11	−0.1583 (3)	0.1191 (7)	0.0127 (4)	4.2 (2)	H15B	0.030	−0.130	0.245	5.0*
C12	−0.1560 (4)	−0.1055 (6)	−0.0971 (4)	3.9 (1)	H15C	0.083	−0.060	0.196	5.0*
C13	−0.0512 (3)	−0.3040 (6)	−0.0538 (4)	3.7 (1)	H16A	−0.100	0.192	0.145	5.0*
C14	0.0433 (3)	−0.2820 (6)	0.0996 (4)	3.5 (1)	H16B	−0.074	0.104	0.221	5.0*
C15	0.0372 (3)	−0.0601 (7)	0.2084 (4)	3.6 (1)	H16C	−0.022	0.181	0.174	5.0*
C16	−0.0637 (3)	0.1346 (7)	0.1679 (4)	4.3 (2)	H31A	0.678	0.131	0.010	5.0*
C21	0.6057 (3)	0.0308 (5)	0.0630 (4)	2.4 (1)	H31B	0.624	0.219	0.047	5.0*
C22	0.6058 (3)	−0.0730 (5)	0.0045 (4)	2.8 (1)	H31C	0.682	0.152	0.108	5.0*
C23	0.5631 (3)	−0.1797 (5)	0.0114 (3)	2.7 (1)	H32A	0.648	−0.148	−0.093	5.0*
C24	0.5198 (3)	−0.1827 (5)	0.0733 (3)	2.7 (1)	H32B	0.647	0.002	−0.095	5.0*
C25	0.5196 (3)	−0.0808 (5)	0.1301 (3)	2.8 (1)	H32C	0.701	−0.071	−0.032	5.0*
C26	0.5621 (3)	0.0254 (6)	0.1259 (3)	2.8 (1)	H33A	0.534	−0.355	−0.035	5.0*
C31	0.6517 (3)	0.1433 (6)	0.0563 (4)	4.1 (1)	H33B	0.554	−0.263	−0.105	5.0*
C32	0.6542 (4)	−0.0725 (7)	−0.0601 (4)	4.4 (2)	H33C	0.611	−0.327	−0.042	5.0*
C33	0.5660 (3)	−0.2908 (6)	−0.0477 (4)	3.5 (1)	H34A	0.447	−0.284	0.126	5.0*
C34	0.4749 (4)	−0.2979 (6)	0.0808 (4)	4.2 (2)	H34B	0.445	−0.309	0.029	5.0*
C35	0.4724 (4)	−0.0808 (7)	0.1982 (4)	4.5 (2)	H34C	0.502	−0.372	0.092	5.0*
C36	0.5639 (4)	0.1330 (7)	0.1880 (4)	4.3 (2)	H35A	0.480	−0.004	0.231	5.0*
C41	−0.2573 (3)	−0.1644 (6)	0.1505 (4)	3.5 (1)	H35B	0.426	−0.085	0.173	5.0*
C42	−0.3408 (3)	−0.2819 (6)	0.2133 (3)	2.9 (1)	H35C	0.482	−0.154	0.234	5.0*
C43	−0.2818 (3)	−0.2843 (5)	0.1764 (3)	2.7 (1)	H36A	0.596	0.196	0.174	5.0*
C44	−0.2462 (3)	−0.3962 (6)	0.1675 (3)	2.9 (1)	H36B	0.520	0.170	0.187	5.0*
C45	−0.1747 (3)	−0.3906 (5)	0.1578 (3)	2.5 (1)	H36C	0.579	0.099	0.244	5.0*

[a] Parameters with an asterisk were refined isotropically.

Table IV. Electrochemical and Spectroscopic data for Organometallic Superionic Donor-Acceptor Complexes

complex	λ_{max}	$h\nu_{CT}$, eV	ν_{CN}	cation	$E^{\circ(2+/1+)}$, V vs SCE
1a	500	2.48	2167, 2180	$(C_6Me_6)_2Fe^{2+}$	−0.24
1b	531	2.28	2170, 2184	$(C_6H_3Me_3)_2Fe^{2+}$	+0.02[a]
2a	380	3.24	2166, 2180	$(C_6Me_6)_2Ru^{2+}$	−1.01
2b	400	3.10	2171, 2186	$(C_6H_3Me_3)_2Ru^{2+}$	−0.75[a]
$[n\text{-}Bu_4N^+]_2[iso\text{-}C_4(CN)_6^{2-}]$			2158, 2173		+0.92[b] (2−/1−)
$[n\text{-}Bu_4N^+]_2[C_6(CN)_6^{2-}]$			2163, 2181		+0.43 (2−/1−)
$[(C_6H_3Me_3)_2Fe^{2+}][C_6(CN)_6^{2-}]$[6a]	730	1.69	2169, 2189		
$[(C_6Me_6)_2Fe^{2+}][C_6(CN)_6^{2-}]$[6a]	800	1.55	2169, 2188		
$[(C_6H_3Me_3)_2Ru^{2+}][C_6(CN)_6^{2-}]$[6a]	503	2.46	2170, 2189		
$[(C_6Me_6)_2Ru^{2+}][C_6(CN)_6^{2-}]$[6a]	540	2.30	2170, 2187		

[a] Since the reversible redox potentials for these cations could not be determined due to the irreversible nature of the reduction, ΔE_{redox} was estimated from the difference in the peak potentials. The difference is equivalent to ΔE_{redox} for the $(\eta^6\text{-}C_6Me_6)_2M^{2+}$ cations, and therefore the use of peak potentials appears valid. [b] $E_{p/2}$ for the irreversible $[C_4(CN)_6]^{2-}/[C_4(CN)_6]^{1-}$ couple.

contribution of D^-A^+ term to the ground state. Unfortunately, the unstable nature of the radical monoanion precludes experimental determination of ν_{CN} for this species, and therefore estimates of the degree of charge transfer in this manner are not possible. Regardless, it is interesting to note that the essentially identical values of ν_{CN} observed for **1a,b** and **2a,b** are not consistent with the different electron affinities of the cations, as a greater extent of mixing would be expected when M = Fe owing to its larger electron affinity. This suggests that the shifts in ν_{CN} may be primarily due to the close interstack contacts between the anion nitrogen atoms and hexamethylbenzene ligands and the resulting electrostatic effects. Similar conclusions were reached for $[(C_6Me_3H_3)_2M^{2+}]\{C_3[C(CN)_2]_3^{2-}\}$.[6a] Although it may be argued that the effect of different electron affinities on vibrational frequencies is too small to be observed, these results illustrate that caution must be exercised when evaluating the extent of excited-state mixing from vibrational frequencies in DA solids.

Single-Crystal Structure of $[(C_6Me_6)_2Fe^+][PF_6^-]$. Single-crystal X-ray structural studies of $[(C_6Me_6)_2Fe^+][PF_6^-]$ (**3**) revealed that this compound crystallized in the orthorhombic space group *Pnnm*, with chains of $(C_6Me_6)_2Fe^+$ cations and PF_6^- anions (Figure 6). The 19e radical cation is structurally similar to the dica-

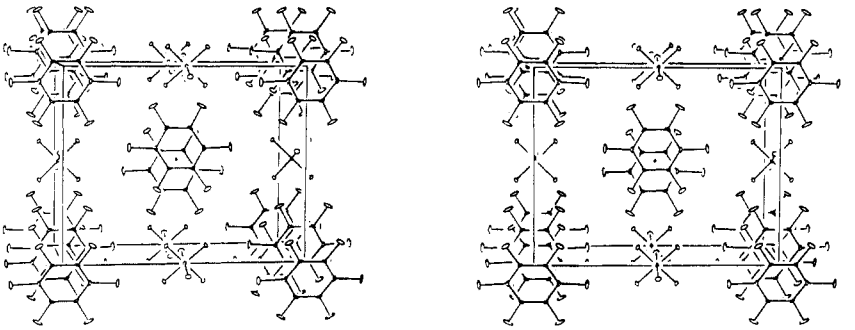

Figure 6. Stereoview of the unit cell of **3**. Atoms are drawn with 50% elipsoids.

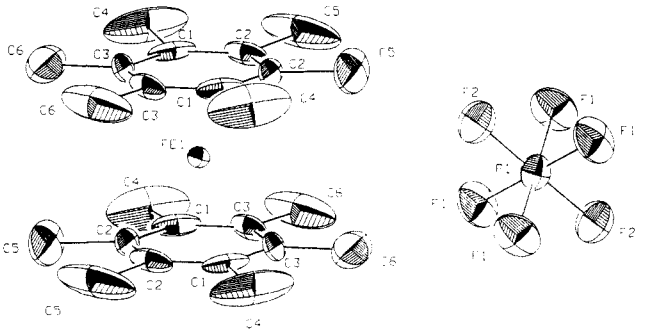

Figure 7. ORTEP drawing of the $(C_6Me_6)_2Fe^+$ and PF_6^- ions in **3**.

Table V. Intramolecular Bond Distances (Å) in $[(C_6Me_6)_2Fe^+][PF_6^-]$ (3)[a]

atoms		distance
Fe1	C1	2.174 (8)
Fe1	C2	2.177 (8)
Fe1	C3	2.184 (8)
P1	F1	1.587 (5)
P1	F2	1.585 (7)
C1	C2	1.413 (12)
C1	C3	1.388 (11)
C1	C4	1.530 (11)
C2	C2a	1.364 (19)
C2	C5	1.530 (12)
C3	C3a	1.387 (17)
C3	C6	1.470 (12)

[a] Numbers in parentheses are estimated standard deviations in the least significant digits.

tion, with mutually parallel C_6Me_6 ligand planes and no extraordinary bond length distortions (Tables V and VI, Figure 7). The average $Fe-C_{ring}$ distance is 2.178 (8) Å, while the average $C_{ring}-C_{ring}$ and $C_{ring}-C_{methyl}$ distances are 1.388 (19) and 1.510 (12) Å, respectively. The intramolecular interplanar separation between the ligands is 3.351 Å, which is slightly larger than that observed in the dication. The larger interligand separation and $Fe-C_{ring}$ distances in **3** compared to $(C_6Me_6)_2Fe^{2+}$ suggests population of Fe–ligand antibonding orbitals, which is consistent with previous reports that indicate mixing of the metal and ligand orbitals in the LUMO of $(C_6Me_6)_2Fe^{2+}$.[26-29]

Since the CT transition in these solids is tantamount to oxidation of the dianions and reduction of the dications, the conformational requirements of the molecular constituents in the excited state can be elucidated from the structure of the $(C_6Me_6)_2Fe^+$ and the polycyano monoanions. The absence of any severe distortions of $(C_6Me_6)_2Fe^+$ compared to the dication suggests that population of the excited state in the solid state occurs with minimal destabilization of the organometallic cation. Additionally, recent structural investigations of DA solids that incorporate the $C_3[C(CN)_2]_3^{2-}$ radical anion indicate no significant differences in its structural features compared to the dianion,[6b,36] suggesting that the structure of anion in the excited state of $[(arene)_2M^{2+}]\{C_3[C(CN)_2]_3^{2-}\}$ need not differ significantly from that in the ground state. Unfortunately, the structure of the *iso*-$C_4(CN)_6^-$ radical monoanion is not known due to its instability, and it is therefore not possible to comment in this regard. However, it is reasonable to suggest that the lowest energy conformation of the radical monoanion would be similar to that of the dianion owing to the significant steric interactions of the cyano groups. It is therefore apparent that energetically unfavorable molecular conformations can be obviated upon excitation from the $D^{2+}A^{2-}$ ground state to the D^+A^- excited state in this series of complexes.

Table VI. Positional and Isotropic Thermal Parameters for 3

atom	x	y	z	B(iso), Å²
Fe1	5000	5000	5000	1.3 (1)
P1	0	0	5000	3.1 (2)
F1	483 (7)	−980 (5)	4183 (4)	5.2 (2)
F2	1888 (10)	483 (7)	5000	5.7 (3)
C1	6891 (11)	4308 (11)	6015 (6)	3.4 (3)
C2	6184 (10)	3305 (8)	5500 (7)	3.6 (3)
C3	7583 (11)	5295 (7)	5509 (6)	2.9 (3)
C4	6970 (15)	4259 (15)	7136 (7)	9.8 (6)
C5	5485 (14)	2177 (11)	6036 (13)	12.0 (6)
C6	8326 (13)	6330 (11)	6052 (11)	9.0 (5)
H4	7682	4872	7376	8.0
H4′	7397	3461	7328	8.0
H4″	5862	4345	7397	8.0
H5	5993	1460	5791	8.0
H5′	4314	2153	5983	8.0
H5″	5791	2258	6727	8.0
H6	8928	6844	5616	8.0
H6′	9074	6019	6541	8.0
H6″	7450	6786	6361	8.0

Concluding Remarks

The organometallic DA solids described here demonstrate that the design of donor–acceptor complexes need not invoke components with planar molecular structures, as face-to-face stacking of π-networks is not required for charge-transfer behavior. These complexes also lend insight into the electronic properties and solid-state structural aspects of DA solids with unusual, highly charged ground states, which are not commonly observed in either organic or organometallic systems due to the paucity of stable, highly charged species. The isomorphism present for complexes with isostructural $(arene)_2M^{2+}$ dications allows rational modification of the microscopic optical properties of the DA solids by altering the electron affinity of the organometallic acceptor species through homologous substitution of the metal atom. Indeed, for a given donor dianion the CT transition energy for dications with iden-

(36) Ward, M. D.; Fagan, P. J. *J. Am. Chem. Soc.*, in press.

Table VII. Experimental Details for $[(C_6Me_6)_2M^{2+}][iso\text{-}C_4(CN)_6^{2-}]$ Complexes

	1a	2a	3
mol formula	$C_{35}H_{39}FeN_7O_2$	$C_{35}H_{39}RuN_7O_2$	$C_{24}H_{36}FePF_6$
fw	645.59	690.82	525.38
cryst dimens, mm	0.28 × 0.40 × 0.47	0.22 × 0.38 × 0.43	0.28 × 0.07 × 0.77
peak width at half-height	0.48	0.58	0.12
source	Mo Kα (λ = 0.71073 Å)	Cu Kα (λ = 1.54184 Å)	Mo Kα (λ = 0.71073 Å)
temp, °C	−25(1)	−40(1)	−70
space group	monoclinic, $P2_1/c$	monoclinic, $P2_1/c$	orthorhombic, *Pnnm* (No. 58)
a, Å	19.875 (6)	19.973 (2)	7.921 (1)
b, Å	10.512 (2)	10.553 (2)	10.867 (1)
c, Å	15.981 (4)	16.144 (1)	13.632 (1)
β, deg	96.65 (3)	96.80 (7)	
V, Å^3	3316 (3)	3378 (4)	
Z	4	4	2
D(calcd), g/cm^3	1.29	1.36	1.487
abs coeff (μ), cm^{-1}	4.9	41.5	7.64
attenuator	Zr foil, factor 21.1	Ni foil, factor 19.4	not used
scan type	ω–θ	ω–θ	ω–θ
scan rate, deg/min	3–5 (in ω)	3–7 (in ω)	1.7–5 (in ω)
scan width, deg	1.2 + 0.140 tan θ	1.0 + 0.140 tan θ	1.0 + 0.140 tan θ
max 2θ, deg	44.0	110.0	55
no. of refl. measd	4459 total, 3882 unique	4658 total, 4002 unique	1609 total, 1398 unique
correctns	Lorentz–polarization linear decay (from 0.941 to 1.035 on *I*) *reflection averaging* (agreement on *I* = 1.3%)	Lorentz–polarization linear decay (from 0.862 to 1.176 on *I*) *reflection averaging* (agreement on *I* = 1.8%)	Lorentz–polarization no decay
reflctns included	2417 with $F_o^2 > 3.0\sigma(F_o^2)$	2886 with $F_o^2 > 3.0\sigma(F_o^2)$	470 with $I > 3.0\sigma(I)$
parameters refined	389	389	78
unweighted agreement factor	0.061	0.070	0.055
weighted agreement factor	0.080	0.068	0.051
esd of observn of unit weights	2.09	3.04	1.43
convergence, largest shift	0.10σ	0.03σ	0.00
high peak in final diff map, e/Å^3	0.73 (7)	1.38 (12)	0.040

tical ligand environments can be predicted from conveniently measured reduction potentials due to equivalent solvation energies of the different dications and negligible differences in the electrostatic lattice energies of solids comprising these components. The ability to modify the electronic properties of molecular solids in this fashion suggests that design of materials with desired properties can be accomplished by rational approaches.

Experimental Section

Materials. Acetonitrile was distilled from CaH_2 under nitrogen and nitromethane from $CaSO_4$ under nitrogen. Literature methods were used for the preparation of $[(arene)_2Fe^{2+}][PF_6^-]_2$,[37] $[(arene)_2Ru^{2+}][BF_4^-]_2$,[38] and $[n\text{-}Bu_4N^+]_2[iso\text{-}C_4(CN)_6^{2-}]$.[15] Preparation of $[(C_6Me_6)_2Fe^+][PF_6^-]$ was accomplished by Na/Hg reduction of $[(C_6Me_6)_2Fe^{2+}][PF_6^-]_2$ in glyme according to a previously reported procedure.[39]

Equipment. All manipulations were performed under inert-atmosphere conditions using either purified nitrogen or a Vacuum Atmospheres glovebox. Infrared spectra were recorded on a Nicolet 7199 Fourier transform spectrometer. UV–visible diffuse reflectance spectra were recorded on a Cary 2390 spectrometer.

Synthesis of $[(C_6Me_6)_2Fe^{2+}][iso\text{-}C_4(CN)_6^{2+}]$ (1a). Under nitrogen, a solution of $[(C_6Me_6)_2Fe^{2+}][PF_6^-]_2$ (67 mg, 0.1 mmol) in 10 mL of acetonitrile was slowly added to solution of $[n\text{-}Bu_4N^+]_2[iso\text{-}C_4(CN)_6^{2-}]$ (68 mg, 0.1 mmol) in 10 mL of acetonitrile, upon which a magenta precipitate was immediately observed. Filtration of the mixture followed by several washings with acetonitrile gave **1a** in quantitative yield. Anal. Calcd: C, 68.86; H, 6.21; N, 14.38. Found: C, 68.30; H, 6.18; N, 15.04. Similar procedures were used for the preparation of $[(C_6Me_3H_3)_2Fe^{2+}][iso\text{-}C_4(CN)_6^{2-}]$ (**1b**) using $[(C_6Me_3H_3)_2Fe^{2+}][PF_6^{2-}]_2$ (59 mg, 0.1 mmol). Anal. Calcd: C, 67.21; H, 4.83; N, 16.79. Found: C, 66.12; H, 4.84; N, 16.40.

Synthesis of $[(C_6Me_6)_2Ru^{2+}][iso\text{-}C_4(CN)_6^{2+}]$ (2a). Under nitrogen, a solution of $[(C_6Me_6)_2Ru^{2+}][BF_4^-]_2$ (67 mg, 0.1 mmol) in 10 mL of acetonitrile was slowly added to solution of $[Bu_4N^+]_2[iso\text{-}C_4(CN)_6^{2-}]$ (68 mg, 0.1 mmol) in 10 mL of acetonitrile, upon which an yellow precipitate was immediately observed. Filtration of the mixture followed by several washings with acetonitrile gave **2a** in quantitative yield. Anal. Calcd: C, 63.85; H, 5.76; N, 13.34. Found: C, 63.12; H, 5.68; N, 13.74. Similar procedures were used for the preparation of $[(C_6Me_3H_3)_2Ru^{2+}][iso\text{-}C_4(CN)_6^{2+}]$ (**2b**) using $[(C_6Me_3H_3)_2Ru^{2+}][BF_4^-]_2$ (51 mg, 0.1 mmol). Anal. Calcd: C, 60.64; H, 4.43; N, 15.40. Found: C, 59.96; H, 4.52; N, 14.42.

Procedures for Crystal Growth. Crystals for single-crystal X-ray structure determinations were prepared by slow diffusion techniques in three-chambered cells in which the chambers were separated by medium porosity fritted glass. Crystal growth was accomplished with either acetonitrile or nitromethane as solvent, although the latter generally yielded crystals of higher quality. The following procedure for the synthesis of **1a** is exemplary. Nitromethane solutions containing 0.01 M $[(C_6Me_6)_2Fe^{2+}][PF_6^-]_2$ and 0.01 M $[Bu_4N^+]_2[iso\text{-}C_4(CN)_6^{2-}]$ were added to the separate outer compartments of a three-chambered cell. Neat solvent was then added to the center chamber. After the cell was left to stand for 2 weeks at 10 °C under nitrogen, violet needles of **1a** were harvested from the center chamber and washed with nitromethane.

X-ray Data Collection and Data Reduction.[40] Preliminary examination and data collection for **1a**, **2a**, and **3** were performed on an Enraf-Nonius CAD4 computer-controlled κ axis diffractometer equipped with a graphite crystal, incident beam monochromator. Table VII summarizes the relevent conditions of data collection. Cell constants and an orientation matrix for data collection were obtained from least-squares refinement, using the setting angles of 23 reflections in the range $9 < \theta < 14°$ for **1a** and 25 reflections in the range $15 < \theta < 27°$ for **2a**, measured by the computer-controlled diagonal-slit method of centering. As

(37) Helling, J. F.; Braitsch, D. M. *J. Am. Chem. Soc.* **1970**, *92*, 7207.
(38) Bennett, M. A.; Matheson, T. W. *J. Organomet. Chem.* **1979**, *175*, 87.
(39) (a) Michaud, P.; Mariot, J.-P.; Varret, F.; Astruc, D. *J. Chem. Soc., Chem. Commun.* **1982**, 1383.
(40) These services were performed by Oneida Research Services, Inc. (**1a**, **2a**) and J.C.C. (**3**).

a check on crystal and electronic stability three representive reflections were measured every 30 min. The intensities of these standards remained constant within experimental error throughout data collection for **1a**. Linear corrections for decay were applied as given in Table VII.

Structure Solution and Refinement. Relevent conditions are summarized in Table VII. The structures were solved by either direct or Patterson methods. The structures were refined in full-matrix least-squares where the function minimized was $\sum w(|F_o| - |F_c|)^2$, and the weight w is defined as $4F_o^2/s^2(F_o^2)$. The standard deviation on intensities $s^2(F_o^2) = [S^2(C + R^2B) + (pF_o^2)^2]/Lp^2$ where S is the scan rate, C is the total integrated peak count, R is the ratio of scan time to background counting time, B is the total background count, Lp is the Lorentz-polarization factor, and the parameter p (ignorance factor) is a factor introduced to downweight intense reflections. Here p was set to 0.060. Hydrogen atoms were included as fixed atoms in idealized positions.

Scattering factors were taken from Cromer and Waber.[41] Anomalous dispersion effects were included in F_c;[42] the values for $\Delta f'$ and $\Delta f''$ were those of Cromer.[43] Only the reflections having intensities greater than 3.0 times their standard deviation were used in the refinements. The final cycle of refinement converged with unweighted and weighted agreement factors of according to $R_1 = \sum||F_o| - |F_c|/\sum|F_o$ and $R_2 = (\sum w(|F_o| - |F_c|)^2/\sum wF_o^2)^{1/2}$. The height of the highest peak in the final difference Fourier and the estimated error based on ΔF[44] are given in the Table VII. Plots of $\sum w(|F_o| - |F_c|)^2$ versus $|F_o|$, reflection order in data collection, sin (q/l), and various classes of indices showed no unusual trends for any of the compounds.

Acknowledgment. We acknowledge the technical assistance of E. J. Delawski.

Registry No. 1a, 118376-71-9; **1b**, 118376-74-2; **2a**, 118376-73-1; **3**, 53382-61-9; $[Bu_4N^+]_2[C_4(CN)_6^{2-}]$, 118376-69-5; $[Bu_4N^+]_2[C_6(CN)_6^{2-}]$, 58619-43-5; $[(C_6H_3Me_3)_2Fe^{2+}][C_6(CN)_6^{2-}]$, 106865-37-6; $[(C_6Me_6)_2Fe^{2+}][C_6(CN)_6^{2-}]$, 106865-38-7; $[(C_6H_3Me_3)_2Ru^{2+}][C_6(CN)_6^{2-}]$, 106865-39-8; $[(C_6Me_6)_2Ru^{2+}][C_6(CN)_6^{2-}]$, 106865-40-1; $[(C_6Me_6)_2Fe^{2+}][PF_6^-]_2$, 53382-63-1; $[(C_6Me_6)_2Ru^{2+}][BF_4^-]_2$, 71861-31-9.

Supplementary Material Available: X-ray structural reports for **1a**, **2a**, and **3** that contain the following: descriptions of experimental procedures for **1a** and **2a** that include data collection, data reduction, and structure solution and refinement, tables of crystal data, intensity measurements, structure solution and refinement, positional and thermal parameters, general temperature factor expressions (U's), bond distances, bond angles, and torsional angles, root-mean-square (rms) amplitudes of thermal vibrations tables of intermolecular N and H contacts for **1a**, **2a**, and **3**, and least-squares planes for **1a**, and drawings of two cations and a single anion with labeling schemes with 25% probability ellipsoids (64 pages); listings of structure factors for **1a**, **2a**, and **3** (30 pages). Ordering information is given on any current masthead page.

(41) Cromer, D. T.; Waber, J. T. *International Tables for X-Ray Crystallography*; The Kynoch Press: Birmingham, England, 1974; Vol. IV, Table 2.2B.
(42) Ibers, J. A.; Hamilton, W. C. *Acta Crystallogr.* **1964**, *17*, 781.
(43) Cromer, D. J. *International Tables for X-Ray Crystallography*; The Kynoch Press: Birmingham, England, 1974; Vol. IV, Table 2.3.1.
(44) Cruickshank, D. W. J. *Acta Crystallogr.* **1949**, *2*, 154.

Stereoselective Vinylic C–H Activation by a Homogeneous Iridium Catalyst

J. W. Faller* and C. J. Smart

Department of Chemistry, Yale University, New Haven, Connecticut 06520

Received April 22, 1988

Vinylic hydrogen–deuterium exchange between a number of terminal olefins and benzene-d_6 is readily catalyzed by $Ir(i\text{-}Pr_3P)_2H_5$. For mono- and disubstituted 1-alkenes H/D exchange is found to be stereoselective, with a preference for activation of the C–H bond trans to the larger substituent at the β-carbon. The degree of stereoselectivity is found to vary with the bulkiness of the β-carbon substituent. Regio- and stereoselectivity are also observed to be independent of the presence of an allylic proton in the substrate, thus indicating that H/D exchange is effected more readily by direct insertion of the catalyst into the vinyl C–H bond than by either reversible π-allyl complex formation or addition of metal hydride to the double bond followed by β-hydride elimination. In addition, for β,β-disubstituted terminal olefins, it is shown that deuteration of the position cis to the larger β-carbon substituent also can occur via a vinyl C–H activation process as well as indirectly via a metal hydride addition–elimination process.

Introduction

Numerous examples of H/D exchange reactions with arenes are catalyzed by transition-metal complexes in homogeneous systems.[1,2] Although observed less frequently, similar H/D exchanges have also been found between vinylic hydrogens and deuterated solvents.[3] Isomerization catalysts also allow incorporation of deuterium into olefins via metal deuteride intermediates. In all of these cases where an M–H(D) is involved in the reaction path, it is frequently assumed that olefinic H/D exchange occurs either via M–D addition to the double bond followed by β-hydride elimination or via reversible allylic proton abstraction to form an η^3-allyl complex of the metal deuteride. We have found that a third mechanism, namely, reversible insertion of a catalytic species into olefinic C–H bonds, is important in at least one group of catalysts, bis(trialkylphosphine)iridium pentahydrides. The relevance of this process may well extend to other

(1) (a) Chatt, J.; Davidson, J. M. *J. Chem. Soc.* **1965**, 483. (b) Parshall, G. W. *Catalysis* **1977**, 334. (c) Barefield, E. K.; Parshall, G. W.; Tebbe, F. N. *J. Am. Chem. Soc.* **1970**, *92*, 5234–5. (d) Jones, W. D. *J. Am. Chem. Soc.* **1984**, *106*, 1650–1663; **1985**, *107*, 620–631 and references therein. (e) Crabtree, R. H. *Chem. Rev.* **1985**, *85*, 245–269 and references therein.
(2) By "catalyst" we mean the compound added to the reaction to accelerate its rate. Important intermediates in the catalytic cycle are referred to as "active" species. [Cf. Tolman, C. A.; Faller, J. W. In *Homogeneous Catalysis with Metal Phosphine Complexes*; Pignolet, L. H., Ed.; Plenum Press: New York, 1983, p 14.]
(3) Cramer, R. *J. Am. Chem. Soc.* **1966**, *88*, 2272; *Acc. Chem. Res.* **1968**, *1*, 186–191.

0276-7333/89/2308-0602$01.50/0